Journal of the European Ceramic Society 8 (1998) 2331–2338
© 1999 Elsevier Science Limited
Printed in Great Britain. All rights reserved
PII: S0955-2219(98)00239-8
0955-2219/99/$—see front matter

Hot-corrosion of Silicon Carbide in Combustion Gases at Temperatures Above the Dew Point of Salts

M. Carruth,[a]* D. Baxter,[a] F. Oliveira[a] and K. Coley†[b]

[a]European Commission–Joint Research Centre, Institute for Advanced Materials, 1755 ZG Petten, The Netherlands
[b]Department of Mechanical Engineering, Strathclyde University, Glasgow, Scotland, UK

Abstract

To evaluate the performance of SiC to operating environments expected in future ceramic gas turbines, SiC samples were exposed in a low velocity burner rig at temperatures above the dew point of sodium sulphate (Na_2SO_4). Under these conditions, the corrosion behaviour should be independent of the sulphur content of the fuel, if $Na_2SO_{4(g)}$ is not involved in the corrosion process. At 1000°C, SiC degradation was dependent on the sulphur levels in the fuel and the rates were controlled by the properties of the glassy corrosion products. Although there was an effect of P_{SO_3} on a_{Na_2O} at 1300°C, the formation of an inner crystalline silica layer protected the material in both combustion gases so that the effect of p_{SO_3} on corrosion was concealed. These results indicate that $Na_2SO_{4(g)}$ is involved in the corrosion process at temperatures above the dew point, contrary to what might be predicted from thermodynamic considerations. The role of sodium on enhancing the rate of corrosion is discussed. © *1999 Elsevier Science Limited. All rights reserved*

1 Introduction

One of the most challenging problems in material science is the development of structural components that can operate well at high temperatures in corrosive environments. Materials are urgently required which can meet this criterion for use in applications such as gas turbines. The introduction of these advanced components will effectively enhance the efficiency of power generation systems, decreasing both the burden on non-renewable fossil fuel resources and the volume of pollutants to the environment. Since metals have practically reached the limit of their high temperature capabilities, special emphasis is placed on the role that ceramics can play in future gas turbine technologies.

Silicon-based ceramics are inherently unstable at high temperatures in air where they oxidise to form silica. Silica has a low oxygen permeability and may, thus, act as an effective barrier to diffusion. The significant improvements made recently in the elevated temperature strength of silicon carbide[1] have increased the amount of attention that this ceramic has been receiving. Silicon carbide is highly regarded as a possible replacement for metals in gas turbines, an application in which ingested airborne contaminants react with the sulphur in the fuel. Under certain conditions, salts form that can condense on turbine components. It is therefore important to assess the effect of these salts on the performance of silicon carbide. Research has now been focused to establish a better understanding of the corrosion behaviour of silicon carbide in gas turbine environments.

Low velocity burner rigs can provide a good understanding of the interaction between ceramic materials and salts at elevated temperatures. Most conditions in a gas turbine can be accurately simulated in a low velocity burner rig, with the exception of gas velocity and pressure.[2] Since the combined effects of oxidation, corrosion and thermal cycling can be simultaneously or independently studied, a low velocity burner rig facility was used in the present work to provide an overall assessment of silicon carbide performance in simulated gas turbine combustion atmospheres.

The most comprehensive burner rig studies have been performed on superalloys at temperatures where salts deposit and react with the protective scale.[3,4] Corrosion rates are observed to increase

*To whom correspondence should be addressed.
†Current address: McMaster University, Hamilton, Canada.

according to the classic Type I hot corrosion process.[5,6] Silicon-based ceramics have been studied under similar conditions and have been shown to follow a comparable corrosion mechanism: deposition of liquid Na_2SO_4 proceeded by dissolution of the silica scale.[7]

Na_2SO_4 forms from fuel impurities and ingested sodium through the reaction:[8]

$$2NaCl_{(g)} + SO_{3(g)} + H_2O_{(g)} = Na_2SO_{4(l)} + 2HCl_{(g)} \quad (1)$$

The melting point of pure Na_2SO_4 is fixed (884°C), but the dew point depends primarily on two factors; the operating pressure and gas composition, namely the sulphur and sodium contents. Operating at atmospheric pressure with 10 ppm Na present in a 0.05% S combustion gas will result in a Na_2SO_4 dew point of 991°C. Increasing the pressure to 5 atmospheres will raise the dew point by 80°C, increasing the risk of deposition.[7]

Silica, being an acidic oxide, has been observed to undergo only basic dissolution.[7] This process can occur following the dissociation of Na_2SO_4 according to:

$$Na_2SO_{4(l)} = Na_2O_{(s)} + SO_{3(g)} \quad (2)$$

When there is a high partial pressure of SO_3 in the gas above the salt at unit activity, a low Na_2O activity [a_{Na_2O}] results. Similarly, a low partial pressure of SO_3 sets a high Na_2O activity. The activity of Na_2O is generally taken as the basicity index so that basic conditions are satisfied for high a_{Na_2O}, which enhances the attack of SiO_2 by sodium via:

$$Na_2O_{(s)} + x.SiO_{2(s)} = Na_2O.x(SiO_2)_{(l)} \quad (3)$$

Thus, corrosion rates may be enhanced by lowering the sulphur content of the fuel.

However, only a limited amount of research has been conducted in the higher temperature regime where developing ceramic gas turbines are expected to operate,[9] i.e. above the dew point of Na_2SO_4. Under these conditions, the corrosion mechanism is expected to be quite different from that described above since no liquid phases are deposited. Thermodynamic calculations predict that the amount of sodium present as NaOH increases above the dew point, and that Na_2SO_4 only exists in small quantities. Thus, the high temperature equivalent of equation (2) should not be important:

$$Na_2SO_{4(g)} = Na_2O_{(g)} + SO_{3(g)} \quad (4)$$

and the a_{Na_2O} may be fixed primarily by:

$$2NaOH_{(g)} = Na_2O_{(g)} + H_2O_{(g)} \quad (5)$$

Since sulphur should not, in principle, directly affect NaOH, corrosion should be independent of p_{SO_3}, unless there is an intermediate reaction occurring where sulphur influences a_{Na_2O}. Performing tests in this high temperature regime, Ahari *et al.*[9] observed a dependence of p_{SO_3} on sodium enhanced corrosion, even at temperatures 200°C above the dew point. This result suggests that there is a reaction occurring at elevated temperatures which involves the control of the Na_2O activity by sulphur.

This study attempts to address the discrepancies that exist between the thermodynamic predictions and the observed corrosion behaviour. By focusing on the overall corrosion process, this investigation searches for a better understanding of the dependence of SO_3 on the sodium enhanced corrosion of SiC.

2 Test material and sample preparation

The corrosion behaviour of a commercially available α-SiC (EKasic D) was used in this investigation. The material was processed using pressureless sintering by ESK (Germany) and samples were supplied as four point bend strength bars, nominal dimensions 3 mm×4 mm×50 mm. The surface roughness (0·25–1.10 μm R_a) depended on the face analysed and the direction in which measurements were made relative to the machining grooves. The oxide thickness and composition on all four sides was the same after exposures in air for 20 h at 1000°C. Thus, differences in surface roughness between the sample faces was not expected to influence the material's corrosion behaviour. The α-SiC grain size varied from about 0·1 to 5 μm. Aluminium, the primary sintering additive, was present in concentrations between 0·67 and 0·74 wt%. X-ray diffraction analysis (XRD) did not identify the presence of free carbon.

In preparation for exposure in the burner rig, the dimensions of each sample were determined to $\pm 1\mu$m at three points along the length using a micrometer. The length was measured to 0·1 mm with a vernier calliper. The samples were ultrasonically cleaned in ethanol, dried and then weighed on a balance accurate to 10 μg.

3 Experimental Procedure and Corrosion Assessment

A low velocity burner rig was used to expose the silicon carbide to various combustion gases. Artificial

ocean water, prepared to ASTM D1141 and then diluted 1:3, was atomised in the rig with 552 $1\,h^{-1}$ of air to achieve a sodium flux of $4\,mg\,cm^{-2}\,h^{-1}$. This contaminant flux rate (CFR) was identical to that used in a round robin program that examined the corrosion of superalloys in burner rigs.[2] However, the CFR is expected not to have the same influence on material degradation when the corrosion mechanism involves transport from the gas phase. Alumina samples were exposed to monitor any salt deposition at the two temperatures studied in this investigation, 1000 and 1300°C, which are both above the dew point of sodium sulphate.

As outlined in the introduction, the primary goal of this exercise was to evaluate the importance of p_{SO_3} on corrosion. Either of two different sulphur containing fuels, a 0·01 wt% S aviation kerosene and a 1 wt% S marine diesel, were injected into the burner rig with a total of 1290 $1\,h^{-1}$ of air. The calculated equilibrium p_{SO_3} in both combustion gases are shown in Table 1. Since thermodynamic calculations using Solgasmix software[10] predict that NaOH is the primary sodium bearing species, the sulphur content of the fuel should neither directly affect a_{Na_2O} (as shown in Table 1) nor corrosion.

The SiC samples stood vertically in a metallic (MA956) sample table, so that the bottom 10 mm of each test bar was not directly exposed to the combustion environment. Alumina crucibles were inserted between the samples and the table to prevent any metal/ceramic interactions occurring at the test temperature. The crucibles also enabled the collection and weight measurement of any low viscosity glasses that flowed down the sample with time. The loaded table was raised into the preheated rig so that the samples were cycled from room temperature to the test isotherm within 20 min. Once the test temperature was reached, peristaltic pumps delivered specific quantities of artificial ocean water and fuel into the rig (50 and $72\,ml\,h^{-1}$, respectively) for 20 h. The table was rotated slowly (~5 rpm) to permit uniform exposure of all sample faces to the combustion gas which was flowing at approximately $0{\cdot}2\,m\,s^{-1}$. After 20 h, the samples were removed from the rig, cooled rapidly in laboratory air and then reweighed. In total, eight thermal cycles were performed for each condition, removing one sample every 40 h to examine the corrosion product. Some samples were analysed by X-ray diffraction (XRD) and then cut 15, 25, 35 and 45 mm from the bottom of the test bar. These cross-sections were prepared for SEM/EDX evaluation.

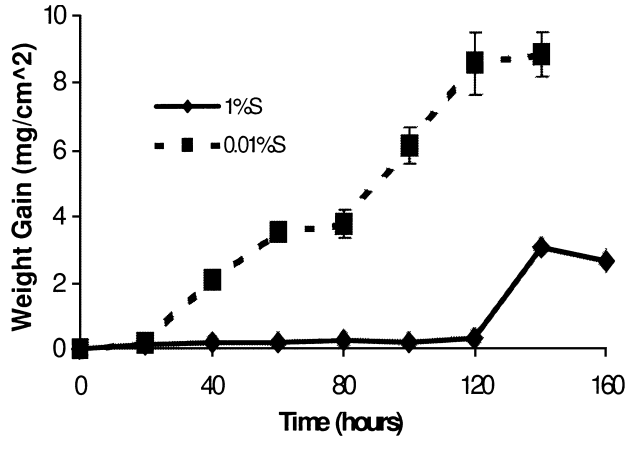

Fig. 1. Average weight gain at 1000°C after each 20 h exposure in the 0·01 wt% S (broken line) and 1 wt% S (solid line) combustion environments. The error bars represent the standard deviation of the measurements.

4 Results

4.1 1000°C

The weight gains of the alumina samples exposed to each fuel at 1000°C were negligible, indicating that no salt deposition had occurred, as expected. The average weight changes of the samples exposed to the two different p_{SO_3} combustion environments at 1000°C are shown in Fig. 1. This data has been corrected to consider the weight gain of the alumina crucibles (due to glass contamination). Due to the test methodology, the weight change plotted over the first two thermal cycles is the average of four samples, and that over the next two thermal cycles is the average of three samples, etc. The average weight gain of the samples exposed to the 0·01 wt% S environment was almost two orders of magnitude greater after 120 h than that determined from the exposure to the 1 wt% S fuel. In fact, the difference in weight gain between the two p_{SO_3} environments was even higher in repeat tests. The low weight increases during the initial and fourth

Table 1. Calculated partial pressures ($kg\,s^{-2}\,m^{-1}$) of some species in the combustion gases simulated in this investigation

	Fuel S content					
	0·01 wt% S			*1 wt% S*		
Temp. (K)	$SO_{3(g)}$	$Na_2O_{(g)}$	$NaOH_{(g)}$	$SO_{3(g)}$	$Na_2O_{(g)}$	$NaOH_{(g)}$
1273	1·01E−02	1·01E−10	3·04E−01	2·03E+00	6·08E−10	2·03E−02
1573	3·04E−03	2·03E−08	1·01E+00	3·04E-01	2·03E-08	1·01E+00

cycles in the 0·01 wt% S fuel are attributed to poor control of the contaminant flux (only ~300 ml of ocean water was injected during these two runs), and highlights the requirement for strict control of the CFR at temperatures even above the dew point of sodium sulphate. However, the low corrosion rates in the 1 wt% S fuel, where the same level of sodium was added, suggests that it is the partial pressures set in the combustion gas, namely p_{SO_3}, that controls corrosion.

A cursory examination of corrosion kinetics suggested that the rate varied linearly with time, a higher rate applied in the lower p_{SO_3} environment. The low weight increase after 140 h was due to an amount of glass that flowed onto the sample table and could not be quantified. This, together with the high weight increase of the alumina crucible, indicates the formation of low viscosity glasses. Note from Fig. 1 that no meaningful weight measurement was obtained after 160 h in the 0·01 wt% S environment since the sample broke on removing from the burner rig. The surface corrosion product however adhered well to the sample and was subsequently analysed.

The corrosion product on the silicon carbide exposed to the 0·01 wt% S fuel consisted of a porous, low viscosity glass that was distributed over the entire sample surface after 80 h. SEM analysis revealed that the thickness of the corrosion product was not uniform. The scale thickness on a sample removed after 40 h varied from 10–70 μm, depending on the face analysed and the section examined. The variation in scale thickness was due to both the formation of a low viscosity corrosion product and a geometry effect. Bubbles were clearly visible in the scale, most probably CO or CO_2 evolved from the oxidation of the SiC. The scale/ceramic interface was generally smooth but some pits were also present. Qualitative chemical analysis by EDX showed that the scales consisted primarily of Si, O, Na and Al. Crystals were observed in the pits and were found to contain only Si and O. These crystals are believed to be cristobalite, which was the only crystalline corrosion product identified by XRD. After 80 h exposure, these crystals had grown from the scale/ ceramic interface to form a semi-continuous layer about 5 μm thick (Fig. 3).

Sections taken from the sample exposed for 140 h showed an increase in scale thickness to ~150 μm. However, there was only limited evidence of cristobalite crystals and these were only present 1 μm into the scale (Fig. 4). The scale thickness had grown to ~200 μm after 160 h and

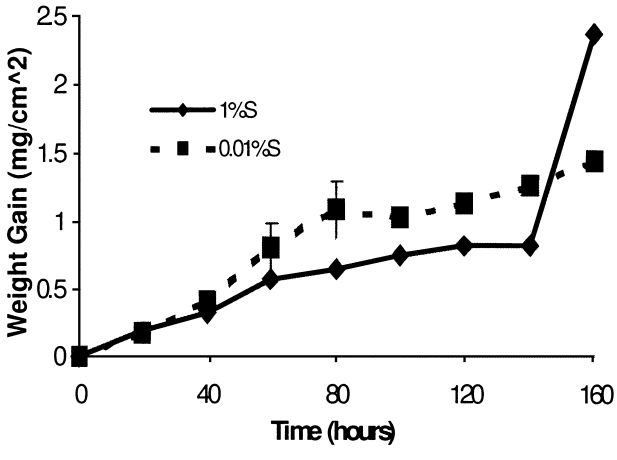

Fig. 2. Average weight gain at 1300°C after each 20 h exposure in the 0·01 wt% S (broken line) and 1 wt% S (solid line) combustion environments. The error bars represent the standard deviation of the measurements.

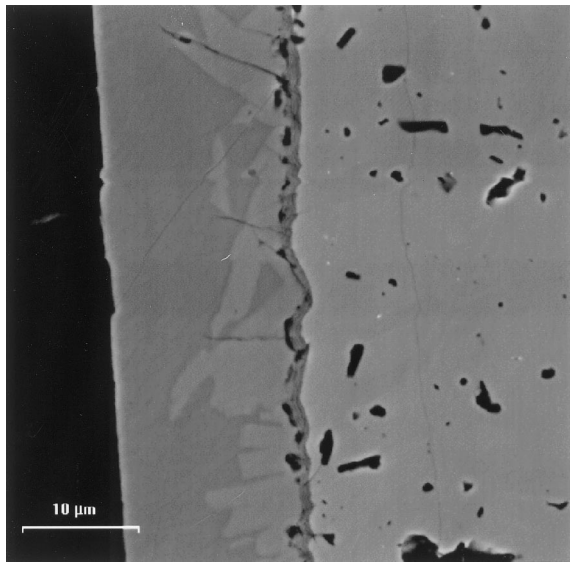

Fig. 3. Section taken 45mm from the sample bottom after 80 h exposure (0·01 wt% S) at 1000°C, highlighting the growth of the silica crystals.

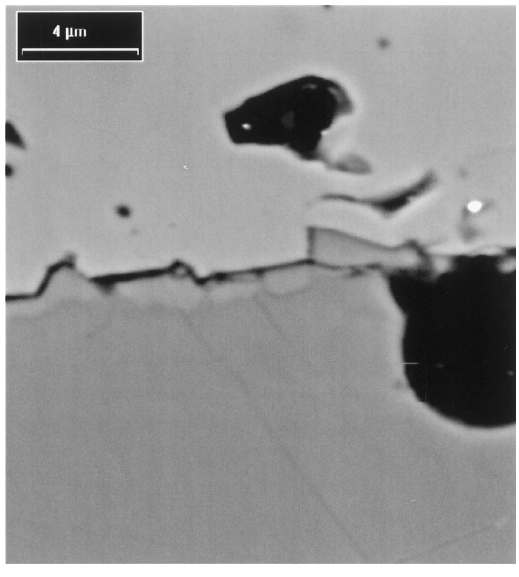

Fig. 4. Section taken 45 mm from the sample bottom after 140 h exposure (0·01 wt% S at 1000°C, showing cristobalite crystals at the oxide/ceramic interface.

there was also evidence of isolated SiC grains in the scale close to the ceramic interface.

The elemental and morphological characteristics of the corrosion products grown on the silicon carbide exposed to the 1 wt% S marine diesel contrasted to that described above. A relatively thin ($\sim 5\,\mu$m) and dense amorphous silica glass had formed on samples exposed for up to 120 h. Only small amounts of sodium and aluminium contamination were identified in the scales and no preferential attack mode was observed at the ceramic/scale interface. Negligible weight increases of the alumina crucibles after six thermal cycles indicated the relatively high viscosity of the corrosion products. However, the sample that had been exposed to the combustion environment for 160 h was coated in a sodium silicate glass of 200 μm thickness in certain places. There was clear evidence of needle-shaped crystals, most probably cristobalite identified by XRD, that appeared to prevent the escape of gas bubbles. The unevenness of the ceramic/scale interface after this exposure period indicated that the silicon carbide degradation was non-uniform, and the relatively high weight increase of the alumina crucibles suggested that the glass was fluid. Repeat tests were performed to determine if these corrosion product features, observed over the last two cycles, were reproducible. The results from this exercise confirmed that the sudden accelerated corrosion was caused by changes in the combustion environment, namely fuel or ocean water fluxes, and that this behaviour was not representative of the materials performance under uniform experimental conditions. Previous experience with burner rig testing has highlighted that unusually high corrosion rates are exhibited when less fuel or excess salt is accidentally injected in to the rig. Furthermore, a separated study performed in this laboratory (as yet unpublished) showed that the corrosion rate decreased markedly when the artificial ocean water was deliberately switched off every alternate thermal cycle.

In an effort to discern the relationship between sulphur and sodium, the corrosion products were characterised by Electron Microprobe Analysis (EPMA). After 40 h, only the corrosion product formed in the 0·01 wt% S fuel environment was thick enough to allow accurate analysis. Silicon and oxygen were evenly distributed throughout the scale, in approximate concentrations of 30 and 70 at%, respectively, indicating that the corrosion product was silica. The results also indicate that the oxide scales were sodium contaminated, with the level of contamination remaining comparable over the test duration. However, a significant difference existed in the level of Na incorporated in the silica oxide formed on the SiC samples exposed to both combustion environments. After 160 h exposure, sodium was present in the silica glass exposed to the 0·01 %wt S in concentrations up to $\sim$5 at%, whereas only 0·1 at% Na was detected in the oxide exposed to the 1 wt% S fuel combustion gas.

4.2 1300°C

The average weight gains of the silicon carbide samples exposed in both combustion environments at 1300°C were comparable, as shown in Fig. 2. A weight gain of $\sim 1\,\mathrm{mg\,cm^{-2}}$ was measured after 120 h in the two different p_{SO_3} gases. Higher weight gains were registered on the alumina crucibles in the 0·01 wt% S fuel gas compared with that measured in the 1 wt% S combustion gas, indicating variations in the viscosity of the corrosion products in both combustion environments. However, the difference was not as great as that observed at 1000°C.

Microstructural analysis indicated that the oxide scales were similar after a specific exposure period in both combustion environments. Figures 5 and 6 highlight the variation in corrosion product morphologies and chemical compositions with time. XRD identified that cristobalite was the primary crystalline corrosion product in all cases, but small quantities of tridymite were also detected. SEM investigation of transverse sections through the scale revealed that the corrosion product thickness increased with time, although the actual thickness depended on the face analysed and the distance along the sample from which the section was taken. Silicon carbide samples removed from the burner rig after 80 h had corrosion products consisting of an inner and an outer layer. The inner layer contained crystals, rich in silicon and oxygen,

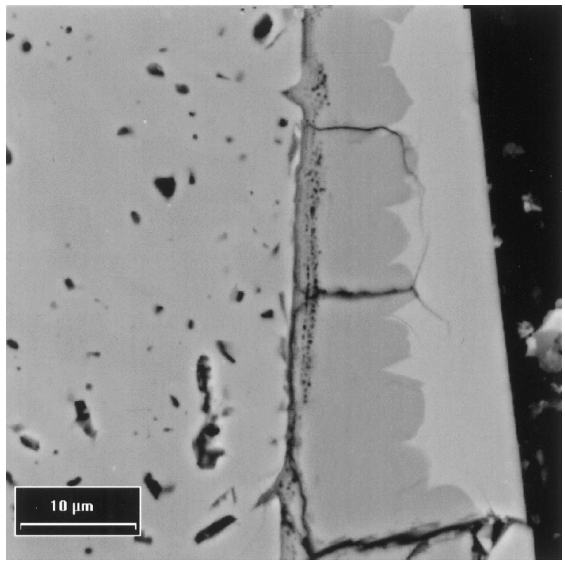

Fig. 5. Section taken 45 mm from the sample bottom after 80 h exposure at 1300°C (1 wt% S), showing silica crystals and silicate glass.

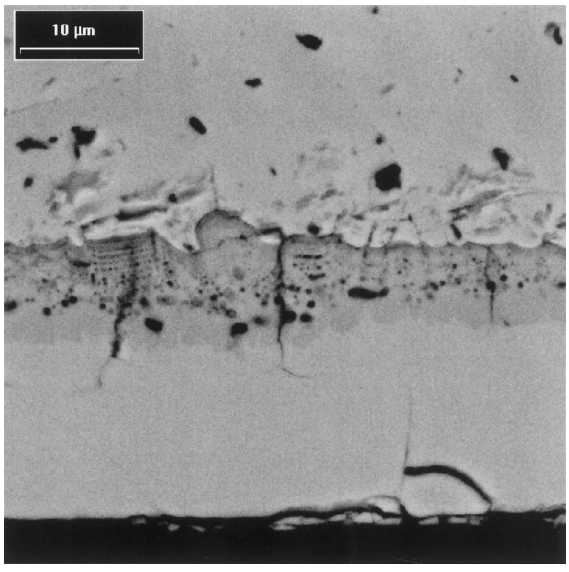

Fig. 6. Section cut 15 mm from the bottom of the sample removed after 160 h (0·01 wt% S) at 1300°C, illustrating the bubble morphology in the inner scale.

which grew outwards from the ceramic/scale interface with time. The outer layer, on the other hand, was amorphous and sodium contaminated.

EPMA results highlighted that the sodium concentrations were higher in the outer scale of samples exposed to the 0·01% S fuel gas. Comparing the concentrations after 160 h, 5 and 12 at% Na was detected in the oxide layer grown in the 1 and 0·01 wt% S environments, respectively. This is consistent with the results at 1000°C that also indicated that the oxide formed in the 0·01 wt% S environment had a higher Na content compared with that formed in the 1 wt% S combustion gas.

5 Discussion

The results show that the corrosion behaviour of silicon carbide is quite complex in simulated gas turbine environments. Under the experimental conditions used in this investigation, the rate of SiC corrosion product formation was substantially greater than that expected from simple oxidation. This suggests that the SiO_2 is being altered, reducing its protective properties and allowing accelerated corrosion to proceed. Alkali contaminants in the gas phase are incorporated in the scale where they change the transport and chemical properties of the corrosion product. The incorporation of sodium in the scale was correlated to higher weight gains, thicker corrosion layers and enhanced corrosion. It would seem unlikely that SiC degradation would depend on p_{SO_3} above the dew point of sodium sulphate, unless there is an influence of sulphur on a_{Na_2O}. In the present study, both thermodynamic calculations and negligible weight gains of the alumina control specimens, indicate that liquid Na_2SO_4 was not present in any of the simulated combustion environments. Therefore, little importance is attached to eqn (2) in these corrosion processes above the dew point, as expected. Also, sulphur contamination was not identified in any of the scales, eliminating a possible direct effect of sulphur on degradation. However, the results show that, at 1000°C, there is a clear influence of p_{SO_3} on corrosion. Higher p_{SO_3} values set lower a_{Na_2O} which fixes acidic conditions and SiO_2 may remain stable. On the other hand, a low p_{SO_3} sets higher Na_{20} activities which results in higher Na concentrations in the glass, thereby reducing the viscosity of the corrosion product and increasing diffusant transport rates. These observations suggest that Na_2SO_4 is still important even when no condensed phase forms. Thus, at 1000°C, eqn (4) appears to play a significant role in the corrosion process, contrary to thermodynamic calculations that predicts a_{Na_2O} to be independent of sulphur (Table 1).

Diffusion of alkali metal ions in vitreous silica is inversely proportional to ionic size,[11] so Na, having a small ionic diameter, would be expected to diffuse quite rapidly towards the SiC. Sodium could then (if the conditions allow) react with the silica to form sodium silicate via eqn (3), lowering the glass viscosity. The result of which is that oxygen diffusion through the glass is accelerated, since it has been shown that atomic oxygen diffusivities, can be six orders of magnitude faster in sodium silicate[12] than in SiO_2 glass[13] and that the addition of network breaking ions, such as sodium, is likely to increase the ionic oxygen diffusion coefficient. Oxygen is then able to react with the SiC at the scale/ceramic interface at a faster rate, forming more silica and CO than under simple oxidation conditions. Since the diameters of CO and O_2 molecules are similar (2·58 and 2·73 Å, respectively), the permeability of CO is expected to be comparable with that of O_2. The presence of more gas bubbles in the scales formed on the samples exposed to the 0·01 wt% S fuel can, therefore, be explained if there is greater influence from ionic diffusion on the degradation process. Also gas permeation is reduced by the incorporation of Na^+ in interstitial sites[14] and, thus, CO bubble formation would be more likely when the rate of corrosion is controlled by ionic diffusion. The faster corrosion when the scales are contaminated with sodium is supported by the work of Babini *et al.*[15] who reported that the contamination of metallic impurities, such as sodium, lowers the viscosity of the glass, promoting ionic diffusion.

There are clear kinetic differences in the oxidation behaviour of the SiC exposed to the two sulphur

fuels at 1000°C. Corrosion in the 1 wt% S combustion environment was affected by changes in the fuel or ocean water fluxes. A decrease in p_{so_3} resulted in an increase in a_{Na_2O} that led to increased Na incorporation in the scale. Since the percentage of Na in the oxide does not change considerably with time under uniform exposure conditions, corrosion is sensitive to the environment's ability to alter Na pick up by the scale. It appears that once a_{Na_2O} is sufficiently high enough to permit a critical level of impurities in the scale to be exceeded (which is less than 0·1 at% Na), the physical properties of the scale are significantly altered to accelerate transport rates. Corrosion is thereby enhanced, due to the increased oxygen transport and other diffusants, through the lower viscosity glass.

The results obtained in the 0·01 %S fuel gas at 1000°C highlight the importance of controlling the amount of Na injected into the rig. The lower quantity of Na injected into the burner rig during the fourth cycle coincided with a decrease in the rate of reaction. This observation may be further explained by considering corrosion to be controlled by diffusion through the cristobalite crystals that formed during this run. Silica crystals were allowed to nucleate and grow probably due to a shift in the glass composition across the Na_2O–SiO_2 liquidus. It has been reported elsewhere[16] that crossing into the two phase region of the phase diagram[17] corresponds to the presence of significant quantities of pure SiO_2, and a decrease in the rate of reaction. Those results were obtained from a study where a single salt coating was applied to the SiC samples before exposure to elevated temperatures. The corrosion route in this investigation may be expected to be quite different since salt was continually injected into the rig. However, under the conditions used in this study, protective silica formation would be more likely if the level of scale contamination is decreased. This result supports the earlier remark that corrosion is sensitive to the environment (p_{so_3}).

The results suggest that once a certain level of scale contamination has been surpassed (which prevents the formation of silica crystals), there is less influence from sodium on corrosion, i.e. uniform corrosion rates as Na contamination continues to increase. Enhanced oxygen transport, either as an ion or molecule, can explain many of the experimental observations and it may also account for the linear kinetics which imply that an interfacial reaction is rate controlling. Sodium contamination of the scale creates diffusion rates that are extremely fast, to the extent that an interfacial reaction is the slowest oxidation step. The linear rate of reaction is in agreement with the work of Mayer and Riley[18] who observed that oxygen diffusion was not affected by changes in the Na_2O–SiO_2 glass composition. However, since corrosion increased with the quantity of Na_2CO_3 applied to the samples, their study highlighted that the activity of Na_2O at the outer surface was a critical parameter in determining degradation.

The similar corrosion rates observed on the SiC exposed to both combustion gases at 1300°C can be attributed to the formation of an inner crystalline silica layer. It appears that this region acts as an effective oxidation barrier, decreasing oxygen diffusion, even when the driving force for silica dissolution by a_{Na_2O} is higher at this temperature. Thermodynamic calculations show that there is no change in a_{Na_2O} in the two combustion gases (Table 1). However, the higher concentration of Na in the samples exposed to the 0·01 wt% S fuel (which resulted in the formation of a lower viscosity glass), suggests that there is still an influence of p_{so_3} on a_{Na_2O}. It is only because corrosion is controlled primarily by the properties of the crystalline SiO_2 layer rather than that of the glass, that the effect of p_{so_3} is concealed. The formation of lower viscosity glasses, caused by the exposure in low p_{so_3} environments, may have an influence on the materials performance if the glass is able to run off the sample surface. This effect might be seen at longer exposure times than those used in this study.

Increasing the temperature should reduce the viscosity of any glassy phases, enhancing the transport properties and the rate of reaction. On the other hand, since Na can promote silica crystallisation, the effect of its incorporation in the scale can be quite complex. However, it appears that a_{Na_2O} does not influence corrosion significantly at 1300°C, since the formation of silica crystals is more influential on corrosion compared with lower viscosity glasses. Therefore, the degradation of SiC is most likely controlled by diffusion through the crystalline layer. This agrees with the kinetic information that shows a decrease in the rate of corrosion with time.

6 Conclusions

The corrosion rate of SiC in simulated combustion environments was enhanced when the corrosion product was contaminated with sodium. p_{so_3} influences a_{Na_2O} at both temperatures studied in this investigation (1000 and 1300°C) to the extent that the level of sodium contamination in the glassy corrosion product was inversely proportional to p_{so_3}. This indicates that $Na_2SO_{4(g)}$ is involved in the corrosion process even at temperatures above the dew point, in the regime where thermodynamic calculations predict that a_{Na_2O} is independent of sulphur.

At 1000°C, corrosion was extremely sensitive to p_{so_3} setting the activity of Na_2O, subsequently influencing the physical and chemical properties of the SiO_2 glass. The faster oxygen transport through the low viscosity corrosion products allowed accelerated corrosion to proceed. It is suggested that the rate of oxygen diffusion is rapid compared with an interfacial reaction, thus explaining the linear kinetics that were observed at this temperature.

At 1300°C, the degradation process was considered to be dictated by the complex effect of sodium in the corrosion product. The formation of an inner crystalline silica layer effectively limited SiC degradation. This layer concealed the effect of p_{so_3} on corrosion, even though p_{so_3} influenced the viscosity of the glass. The rate of corrosion was controlled by oxygen diffusion through the crystalline silica layer meaning that the impact of sodium contamination in the glass was less dominant.

Acknowledgements

The authors would like to thank everybody who made this investigation possible. A special mention is given to Mr A. Zato, who helped perform the burner rig experiments, and Mr P. Frampton, who prepared the samples for corrosion assessment. This work has been carried out within the European Commission's Research and Development program.

References

1. Liu, D. M., Jou, Z. C., Lin, B. W. and Fu, C. T., Microstructure and high temperature strength of pressureless-sintered silicon carbide. *J. Mater. Sci. Lett.*, 1995, **14**, 1327–1328.
2. Nicholls, J. R. and Saunders, S. R., Comparison of hot-salt corrosion behaviour of superalloys in high and low velocity burner rigs. *High Temperature Technology*, 1989, **7**, 193–201.
3. Hancock, P., The use of laboratory and rig tests to simulate gas turbine corrosion problems. *Corr. Sci.*, 1982, **22**, 51–65.
4. Booth, G. and Clarke, R., Evaluation of corrosion resistance of coated superalloys in rig tests. *Materials Science and Technology*, 1986, **2**, 272–281.
5. Baxter, D. J., Jonas, H., Burke, A., Norton, J. F. and Bregani, F., Burner rig hot-salt corrosion of gas turbine superalloys. In *Materials for Advanced Power Engineering, Part II*, ed. D. Coutsouradis. Kluwer Academic, The Netherlands, 1994, pp. 1233–1242.
6. Nishikita, A., Numata, H. and Tsuru, T., Electrochemistry of molten salt corrosion. *Material Science and Engineering*, 1991, **A146**, 15.
7. Jacobson, N. S., Sodium sulfate: Deposition and dissolution of silica. *Oxidation of Metals*, 1989, **31**, 91–103.
8. Kohl, F., Stearns, C. and Fryburg, G., The role of NaCl in flame chemistry, in the deposition process and its reactions with protective oxides. In 4th US/UK Conference on Gas Turbine Materials in a Marine Environment, Washington, DC, 1979, pp. 565–590.
9. Ahari, K. G., Coley, K. S., Baxter, D. J. and Hendry, A., Behaviour of sialons and silicon nitride in burner rig simulated gas turbine atmospheres. In *High Performance Materials*, ed. P. Vincenzini. Techna Srl, Faenza, 1995, pp. 411–420.
10. Eriksson, G., Thermodynamic studies of high temperature equilibria. SOLGASMIX, a computer program for calculation of equilibrium compositions in multiphase systems. *Chemica Scripta*, 1975, **8**, 100–103.
11. Rothman, S. J., Marcuso, T. L., Nowicki, L. L, Baldo, P. M. and McCormick, A. W., Diffusion of alkali ions in vitreous silica. *J. Am. Ceram. Soc.*, 1982, **65**, 578–582.
12. Oishi, Y., Terai, R. and Ueda, H., Oxygen diffusion in liquid silicates and relation to their viscosity. In *Mass Transport Phenomena in Ceramics*, ed. A. Cooper and A. Hever. Plenum Press, New York, 1974.
13. Schaeffer, H. A., Silicon and oxygen diffusion in oxide glasses. In *Mass Transport Phenomena in Ceramics*, ed. A. Cooper and A. Hever. Plenum Press, New York, 1974, pp. 297–310.
14. Shelby, J. E., Helium diffusion and solubility in potassium oxide–silicon dioxide glasses. *J. Am. Ceram. Soc.*, 1974, **57**, 260–263.
15. Babini, G. N., Bellosi, A. and Vincenzini, P., Factors influencing structural evolution in the oxide of hot-pressed Si_3N_4–Y_2O_3–SiO_2 materials. *J. Mater. Sci.*, 1984, **19**, 3487–3497.
16. Jacoboson, N. S., Kinetics and mechanism of corrosion of SiC by molten salts. *J. Am. Ceram. Soc.*, 1986, **69**, 74–82.
17. Kracek, F. C., *J. Phys. Chem.*, 1930, **34**, 1588. (In *Phase Diagrams for Ceramists*, ed. M. K. Reser. American Ceramic Society, 1964).
18. Mayer, M. I. and Riley, F. L., Sodium-assisted oxidation of reaction bonded silicon nitride. *J. Mater. Sci.*, 1978, **13**, 1319–1328.